Quaternary Research (2021), **102**, 205–221
doi:10.1017/qua.2020.123

Research Article

Late Pleistocene–Holocene stress in the South American intraplate evidenced by tectonic instability in central Amazonia

Dilce F. Rossetti[a]*, Francisco H. R. Bezerra[b], Márcio M. Valeriano[a] and Eder Cassola Molina[c]

[a]Instituto Brasileiro de Pesquisas Espaciais–INPE, São José dos Campos-SP, 12245-970 Brazil; [b]Departamento de Geologia, Universidade Federal do Rio Grande do Norte, Natal-RN, 59078-970, Brazil and [c]Instituto de Astronomia, Geofísica e Ciências Atmosféricas, Universidade de São Paulo–USP, Cidade Universitária, São Paulo-SP, 05508-900 Brazil

Abstract

Documenting neotectonic instabilities and determining the style and time of deformation in the vast and difficult to access central Amazonia region is challenging. We focus on these issues by investigating a large area of the Negro River drainage basin, applying morphostructural analysis based on synthetic aperture radar data. The digital elevation models of the C-band Shuttle Radar Topography Mission and the L-band Protection System of Amazonia were used as the database. We also used subsurface magnetic information from the Earth Magnetic Anomaly Grid global model to validate the morphostructures. The results revealed NW-oriented morphostructural lineaments bounding multiple depositional valley fills. These were extensively fragmented to form regularly distributed en échelon rectangular blocks commonly offset horizontally by several kilometers. Strike-slip faults and oblique, either normal or reverse, faults are present. These structures were reactivated along the main NE- and SW-oriented regional structural trends due to N-S-oriented horizontal compression and E-W-oriented horizontal extension in the late Pleistocene and Holocene. The extensive neotectonic faulting results from the interplay of plate motion and Andean uplifting since the late Pleistocene, combined with local stresses.

Keywords: Fluvial valleys, Digital elevation model, Late Pleistocene–Holocene, Intraplate stresses, Neotectonics

(Received 16 January 2020; accepted 4 December 2020)

INTRODUCTION

The notion of neotectonic stability in central Amazonia has changed in the last decades, with increasing evidence of fault reactivation as an important control of ancient and modern Amazonian river systems (e.g., Franzinelli and Latrubesse, 1993; Franzinelli et al., 1999; Costa et al., 2001; Almeida-Filho and Miranda, 2007; Silva et al., 2007; Hayakawa et al., 2010; Rossetti, 2014a, 2014b). Nevertheless, the style and time of deformation remain to be investigated to understand the relationship with regional neotectonic events and determine the stress field in this intracratonic area of the South American plate.

Although intraplate stress has contributed to neotectonic fault reactivations in several intracratonic basins worldwide (e.g., Bosworth, 2008; Braitenberg and Ebbing, 2009), the associated deformation mechanisms are not fully understood (Braiais et al., 2016). Intraplate neotectonics have generally been attributed to thermal subsidence during the quiescence phase following the main rifting (e.g., Maurin and Guiraud, 1993; Moulin et al., 2010). However, this concept has changed with the record of pervasive postrift tectonic activity in many known passive margins (e.g., Gunnel and Fleitout, 2000; Hudec and Jackson, 2002; Doré et al., 2008), which may affect also continental interior areas. This is also the case for the South American plate, which was affected by extensive post-Cretaceous tectonic deformation along both the plate margins to the east and the Andean chain to the west.

An E-W to ESE-WNW subhorizontal compressive stress field has been proposed to explain the style of neotectonic deformation during the postrift history of the South American plate (Riccomini and Assumpção, 1999), which is also in accordance with general information from the World Stress Map (Heidbach et al., 2018). However, the stress field might vary geographically and might also change in style over geologic time. For instance, current numerical models indicate a rotation of the approximately E-W-oriented maximum horizontal compressive stress of the South America plate (e.g., Assumpção, 1992) to a NW-SE-oriented maximum horizontal compression toward Brazilian Amazonia (e.g., Assumpção et al., 2016), which is also in agreement with earthquakes' focal mechanism in this region (Assumpção and Suárez, 1988). This variation in the Amazonian stress field remains to be explained, and it also needs to be clarified whether or not this was a prevalent pattern in the geologic record.

The present work has the main goal of improving the record of late Pleistocene–Holocene deformation in a large area of central Amazonia, northern Brazil, to expand the discussion about the extension of intraplate stress related to the late-stage motion of the South America plate. To address this issue, we selected an area under the influence of the Negro River valley (Fig. 1A–C),

*Corresponding author at: Instituto Brasileiro de Pesquisas Espaciais–INPE, Rua dos Astronautas 1758, São José dos Campos-SP, 12245–970 Brazil.
E-mail address: dilce.rossetti@inpe.br (D.F. Rossetti).

Cite this article: Rossetti DF, Bezerra FHR, Valeriano MM, Molina EC (2021). Late Pleistocene–Holocene stress in the South American intraplate evidenced by tectonic instability in central Amazonia. *Quaternary Research* **102**, 205–221. https://doi.org/10.1017/qua.2020.123

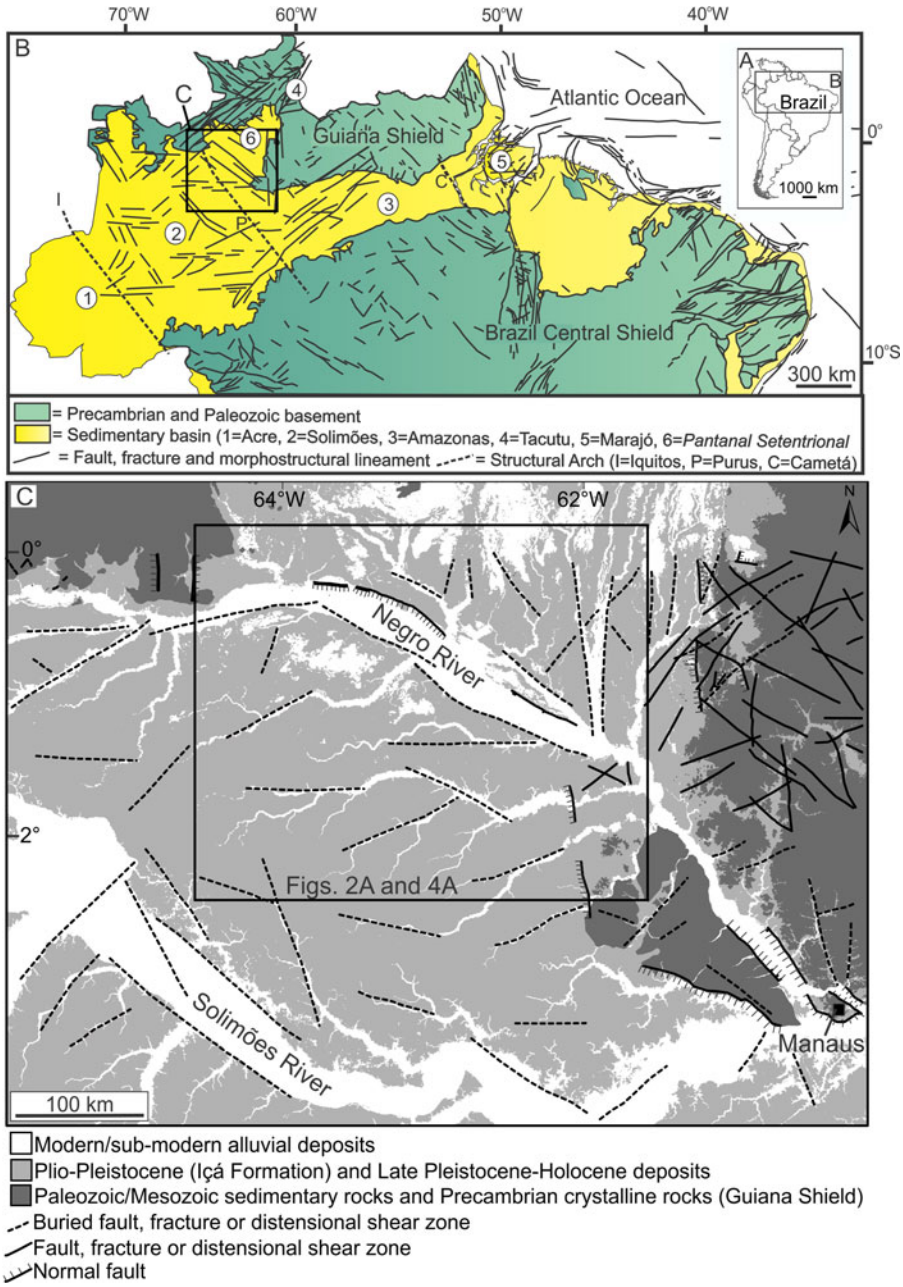

Figure 1. (color online) Location and geologic characteristics of the study area. (A and B) Structural framework in north and northeast Brazil, with indication of main structures that intercept Precambrian shields and sedimentary basins. Also indicated are main fracture zones in the equatorial Atlantic Ocean (modified from Rossetti 2014b). (C) Location of the study area (inside box) along a segment of the Negro River valley, north of central Amazonia. This figure also contains a simplified geologic map with the main lithostratigraphic units found at the surface, as well as main structural features that prevailed over the Precambrian basement and sedimentary basins in the study area and adjacency.

based on its location in a complex tectonic setting, where the main river parallels NW-striking morphostructural lineaments related to major strike-slip faults (Franzinelli and Latrubesse, 1993; Franzinelli and Igreja, 2002; Latrubesse and Franzinelli, 2002).

The present investigation was also motivated by the local finding, on the Negro River left margin, of structures unequivocally related to faults recently reactivated under a right- and left-lateral strike-slip stress regime (Rossetti et al., 2019). Here, we address the impact of the most recent tectonic events on the morphology of the Negro River basin, investigating the trunk valley and some tributaries that drain a vast area north of central Amazonia. Patterns of morphostructural lineaments, corresponding to alignments of drainage systems and relief morphologies, were extracted and compared with regional structural trends. Surface and subsurface magnetometric data were integrated and analyzed in the context of the regional structural framework of central Amazonia.

Using geomorphological criteria, we examined the multistory alluvial fills of the modern valley systems, as well as their frequent partition and lateral displacement as numerous, nearly orthogonal segments. We used these elements to determine the deformation timing, structural style, and stress field regime. These results contribute to the understanding of neotectonic faulting and stresses in the South American intraplate.

PHYSIOGRAPHY AND TECTONO-STRATIGRAPHIC CONTEXT

The Negro River, a main northern tributary of the Amazon River and the longest blackwater river on Earth, has headwaters in Colombia, from whence it flows 2250 km to the confluence with the Solimões–Amazon river systems. The Negro River extends up to 1370 km in the Brazilian territory, frequently changing its orientation and morphology. This river shifts its course

downstream from southeast to east, and then continues southeast as far as its confluence with the Amazon River. After crossing the Precambrian rocks of the Guiana Shield, the Negro River suddenly doubles in width, forming two anomalous segments of approximately 20 km wide in its middle and lower stretches. The study area occurs in the enlarged, upper mid–Negro River valley, including areas drained by several of its tributaries to the south (Fig. 1C).

The study area is geologically located in parts of the Amazonas and Solimões basins, which were established under intraplate extension within the Amazonian Craton (Tassinari et al., 2000). The main sedimentation in these basins was in the Paleozoic. However, renewed deposition occurred during episodes of the Andean Orogeny in the Cretaceous (Alter do Chão Formation) and, in the case of the Solimões Basin, also since the Miocene, being represented by the Solimões and Içá formations (Latrubesse et al., 2010). Deposits mapped as Içá Formation cover most of the study area. This unit, which has a thickness of up to 80 m (Maia et al., 1977; Reis et al., 2006), was originally related to the Plio-Pleistocene, but it also includes several sedimentary successions formed in the Pleistocene and Holocene (Rossetti et al., 2005). Although still open to debate, the northeastern sector of the study area may constitute a separate basin (i.e., the Pantanal Setentrional Basin) formed by Quaternary tectonic reactivation (Rossetti et al., 2016).

An important structure in the studied region is the Purus Arch (Fig. 1B), which is a NW-trending strike-slip fault zone formed along a middle Proterozoic graben inverted in the late Proterozoic and reactivated many times since then, at least up to the late Miocene (Wanderley Filho, 1991; Caputo and Soares, 2016). The Negro River valley in the study area follows this main structural trend, being attributed to a half-graben formed by the reactivation of faults (Franzinelli and Igreja, 2002).

Evidence that the Negro River valley is controlled by tectonics includes numerous drainage anomalies and morphostructural lineaments (Val et al., 2013). An example of anomaly is the megacapture of this river near its confluence with the Solimões River to form the Amazon River. This process also caused tributary systems on the right bank of the Negro River to reverse their flows from south to northeast (Almeida-Filho and Miranda, 2007). In addition, the diverse orientations of the Negro River in the Brazilian territory parallel normal and strike-slip faults, which trend in the main NW and secondary NE, E-W (Franzinelli and Latrubesse, 1993; Latrubesse and Franzinelli, 2002), and N (Latrubesse and Franzinelli, 2005) directions (Figs. 1C and 2A). These structures, which affect both the sedimentary basins and the adjacent Precambrian basement of the cratonic shields (Fig. 1C), parallel regional trends of other areas in the north and northeast of Brazil (Fig. 1B). Furthermore, the seismic anisotropy of the Negro River region trends on an azimuth of 120°, that is, parallel to the direction of the river and of the aeromagnetic anomalies in the area of the Guiana Shield (Rosa et al., 2014). Both geophysical directions are consistent with the regional trends of Proterozoic geologic structures. Focal mechanisms and borehole breakout data available in the World Stress Map (Heidbach et al., 2018) also indicate that the Amazonian region exhibits a NNW-SSE- to NNE-SSW-oriented maximum horizontal stress (Fig. 3). This region represents a different stress province from the equatorial margin and the Andes Cordillera (Assumpção, 1992). Late Pleistocene and Holocene tectonic reactivations along horizontal stress fields were proposed to explain the tectonic structures recorded in different areas of central Amazonia (e.g., Rossetti, 2014a, 2014b), including the region of the Negro River (Val et al., 2013; Rossetti et al., 2019).

The NW-striking midcourse of the Negro River is inverted downstream from north to south, where a dextral strike-slip fault has been inferred (Latrubesse and Franzinelli, 2005; Figs. 1C and 2A). Neotectonic deformation could have caused the reactivation of faults and the displacement of the midcourse of the Negro River to the southwest, a process that resulted in the development of terraces up to approximately 20 km in width on its left bank. Two terraces were recognized in this stretch of the river (Fig. 2B): a topographically high terrace (5 to 9 m) consisting of fluvial silty-clayey sands and massive clays with radiocarbon ages between >40,000 and 27,000 cal yr BP; and a lower terrace (2 to 4 m) consisting of overbank and lateral accretion clays and silts formed between 13,500 and 4000 cal yr BP (Latrubesse and Franzinelli, 2005). In addition, optically stimulated luminescence ages up to 427,000 yrs BP were recorded in sedimentary deposits on the lower reaches of this river (Soares et al., 2010).

MATERIALS AND METHODS

We used the original 3 arc-second (90 m resolution) C-band digital elevation model (DEM) acquired with the interferometric synthetic aperture radar (InSAR) during the Shuttle Radar Topography Mission (SRTM; ftp://e0srp01u.ecs.nasa.gov/srtm, accessed on September 20th, 2020). The 1 arc-second (30 m resolution) DEM of Topodata (Instituto Nacional de Pesquisas Espaciais–INPE, 2008; http://www.dsr.inpe.br/topodata/data/geotiff, access on January 11th, 2021, a full Brazilian topographic coverage database, was also used in this work. Canopy influence in the SRTM-DEM has been noted (Kellndorfer et al., 2004; Walker et al., 2007), but data variations are generally correlated to ground relief on regional scales (Valeriano and Rossetti, 2008, 2017; Polidori and Simonetto, 2014). Our analysis was also improved by using the radar digital elevation model (RDEM) of the Protection System of Amazonia (SIPAM), acquired aboard the R99B shuttle mission. This radar system was operated in the L (23 cm) band, which allowed penetration into the tree canopy to provide ground surface elevations for most of the study area.

The SRTM-DEM and RDEM were processed with custom shading schemes and palettes in the Global Mapper Software (Blue Marble Geographics, Hallowell, ME, USA) to highlight sets of elevation values useful for our analysis. In addition to visual morphological analysis, the DEMs were also the basis for extracting the main morphostructural lineaments, which are straight or gently arched structural lines derived from drainage and relief elements (cf. Holmes, 1965; Howard, 1967; Summerfield, 1991). The morphostructural lineaments were manually vectored, considering lengths ≥2 cm on a fixed scale of 1:100,000. Lineament trends were analyzed with rose diagrams of 10° intervals, considering absolute frequencies (absolute lineament numbers) and absolute lengths (absolute lineament sizes).

In addition to SRTM-DEM and RDEM-DEM, we completed our morphological analysis using high-resolution optical images derived from the free Google Earth (http://www.google.com/earth/index.html, accessed on January 11th, 2021) and WebGLEarth (https://www.bing.com/maps, accessed on January 11th, 2021) catalogs.

The geologic significance of morphostructural lineaments was analyzed by comparison with magnetic lineaments extracted from the Earth Magnetic Anomaly Grid (EMAG2) global model (Maus et al., 2009). This model compiles magnetic data acquired from

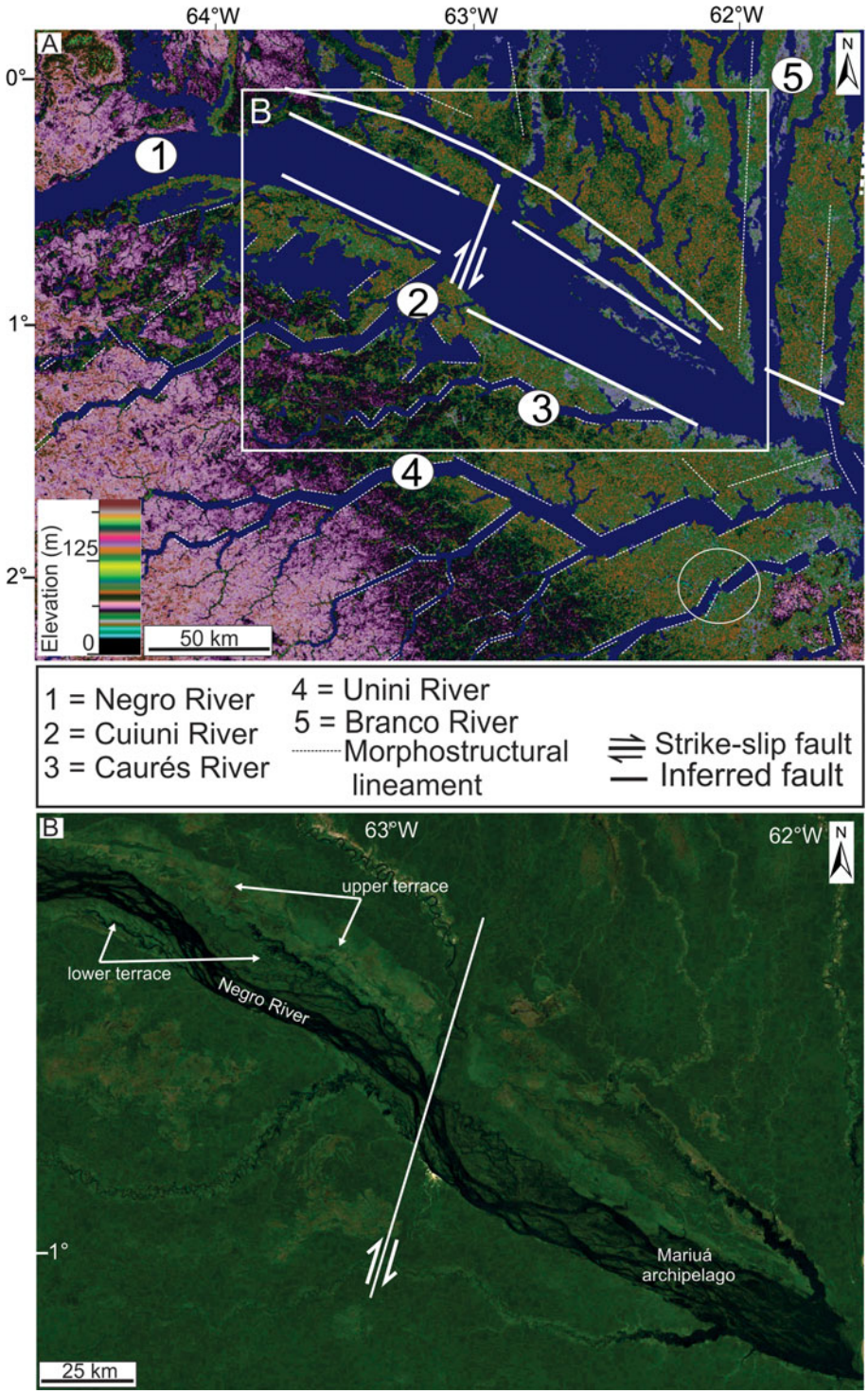

Figure 2. (color online) Regional morphological characteristics of the study area (see also location in Fig. 1C). (A) Main morphostructural lineaments marked on the Shuttle Radar Topography Mission digital elevation model (SRTM-DEM) background, many constituting straight segments with near-orthogonal junctions (circle indicates a place where a tributary channel was laterally displaced by a right lateral strike-slip fault); morphostructural lineaments based on Latrubesse and Franzinelli (2005). (B) The lower and upper terraces of the Negro River on a Google Earth optical image (see location in A).

satellite, marine, and aeromagnetic surveys, calculated at an altitude of 4 km above mean sea level, with a resolution of 2 arc-minute. The grid data were resampled, and a color palette was applied to highlight the magnetic anomalies using the General Mapping Tools software (Wessel et al., 2013).

MORPHOSTRUCTURAL LINEAMENTS

Morphostructural lineaments are abundant across the Negro River valley and its main tributary valleys, where they intercept recent alluvial sediments, as well as interfluvial deposits (Fig. 4A). The extraction of 9373 lineaments in the study area indicated a regional trend of two predominant modes: NW and NE (Fig. 4B); secondary modes trended E and N.

The most remarkable are successions of lineaments, many projecting into older interfluvial Quaternary deposits, which defined laterally displaced rectangular floodplain blocks arranged side by side in en échelon–like pattern. This configuration was particularly well illustrated in three tributaries south of the Negro River: the Cuiuni, Caurés, and Unini. It is worth noting that

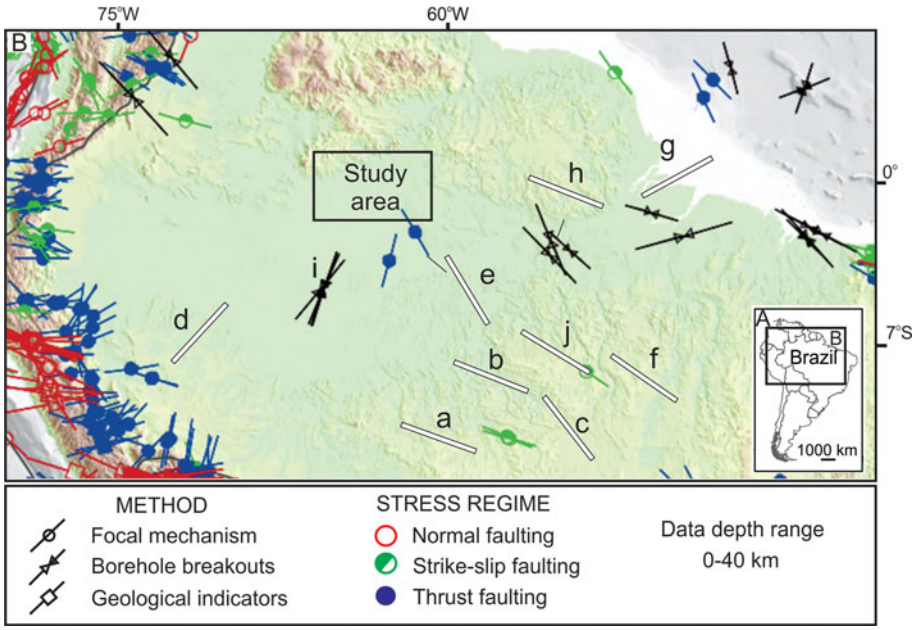

Figure 3. (color online) (A and B) Stress fields for northern South America, with orientation of maximum horizontal compressional stress S_{Hmax}, according to the World Stress Map (cf. Heidback et al., 2018). Also plotted are the stress fields proposed for the Amazonian region, according to: (a–c) Barros et al. (2009); (d and e) Assumpção and Suárez (1988); (f) Assumpção et al. (2016); (g–i) Assumpção et al. (1985); and (j) Ciardelli and Assumpção (2019).

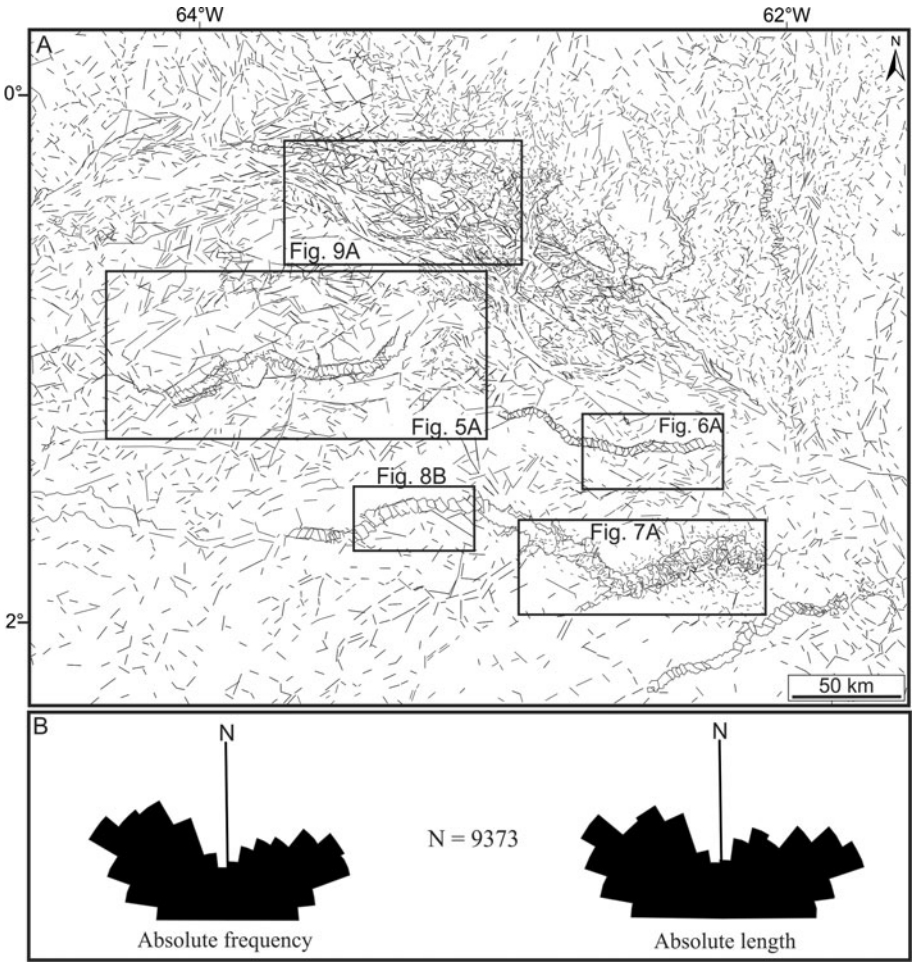

Figure 4. Morphostructural characteristics of the study area (see location in Fig. 1C). (A) Main lineaments extracted from drainage and relief elements derived from the Shuttle Radar Topography Mission digital elevation model (SRTM-DEM) and radar digital elevation model (RDEM). (B) Main structural trends of the lineaments shown in A. The five inserted rectangles indicate the locations shown in Figs. 5A, 6A, 7A, 8B, and 9A, which contain details of selected river valleys with an abundance of fractures, many attributed to strike-slip faults (see text for further explanation).

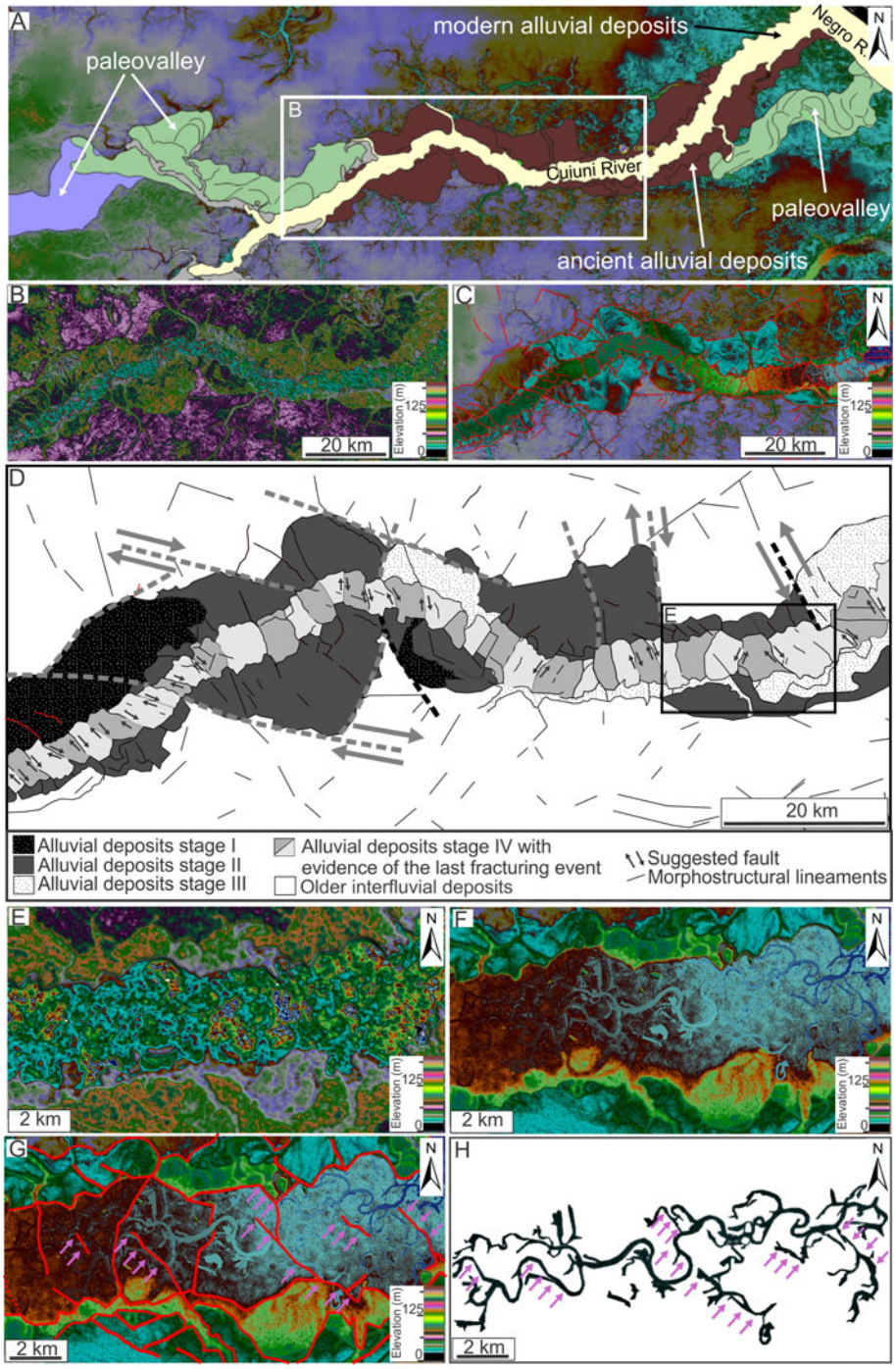

Figure 5. Morphostructural and sedimentary characteristics of the Cuiuni River valley. (A) Alluvial deposits of the ancient and present-day river valley shown on the radar digital elevation model (RDEM) background (see location in Fig. 4A). (B and C) A detail of A, illustrating the curved segment of this river in the Shuttle Radar Topography Mission digital elevation model (SRTM-DEM) (B) and RDEM (C) backgrounds, the latter containing morphostructural lineaments. (D) Enlarged view of C, with the drawing of lineaments bounding floodplain blocks that might be laterally displaced, and plot of sedimentary deposits formed in different stages of the river valley evolution. Note many laterally displaced alluvial deposits bounded by dextral NW- and sinistral NE-striking morphostructural lineaments. The latter consist of a set of successive alignments with planes orthogonal to nearly orthogonal to the main direction of the river valley. The darker and lighter gray colors indicate alternating blocks of stage IV alluvial deposits, laterally displaced and arranged following an en échelon-like pattern. See text for further explanation. (E–G) Detail of a laterally displaced segment of the valley (see location in C) seen on the SRTM-DEM (E) and RDEM (F and G) (with red traces in G highlighting morphostructural lineaments between segmented blocks). (H) Pattern of the modern drainage of the valley segment shown in E–G, with straight channels following morphostructural lineaments (see purple arrows). (For interpretation of the references to color in this figure legend, the reader is referred to the web version of this article.)

these river valleys contained several long segments that are inflected abruptly from NE to NW (Fig. 2A), coincident with the main regional trends.

Cuiuni River

This river changed its location over time, as indicated by a paleovalley morphology remaining on the banks of the modern valley (Fig. 5A). The modern valley exhibits a broad arched shape formed by abrupt and nearly orthogonal segments that separate the paleovalley before the confluence with the Negro River (Fig. 5A–C). The arched stretch of the Cuiuni valley had a complex sedimentary evolution. This is evidenced by the multitemporal fill consisting of at least four stages of successively intercepting floodplain deposits (Fig. 5D), which contributed to progressively downcutting and amplifying the river valley over time. The most notable of stages I to III deposits is the constraint by many straight lineaments with orthogonal junctions (see gray dashed lines in Fig. 5D) that define rectangular to near-rectangular blocks. These are laterally displaced, with offsets up to 9 km (see gray arrows in Fig. 5D). The lineaments either end in these deposits or continue laterally into interfluvial areas and/or floodplain deposits segmented by the stage IV en

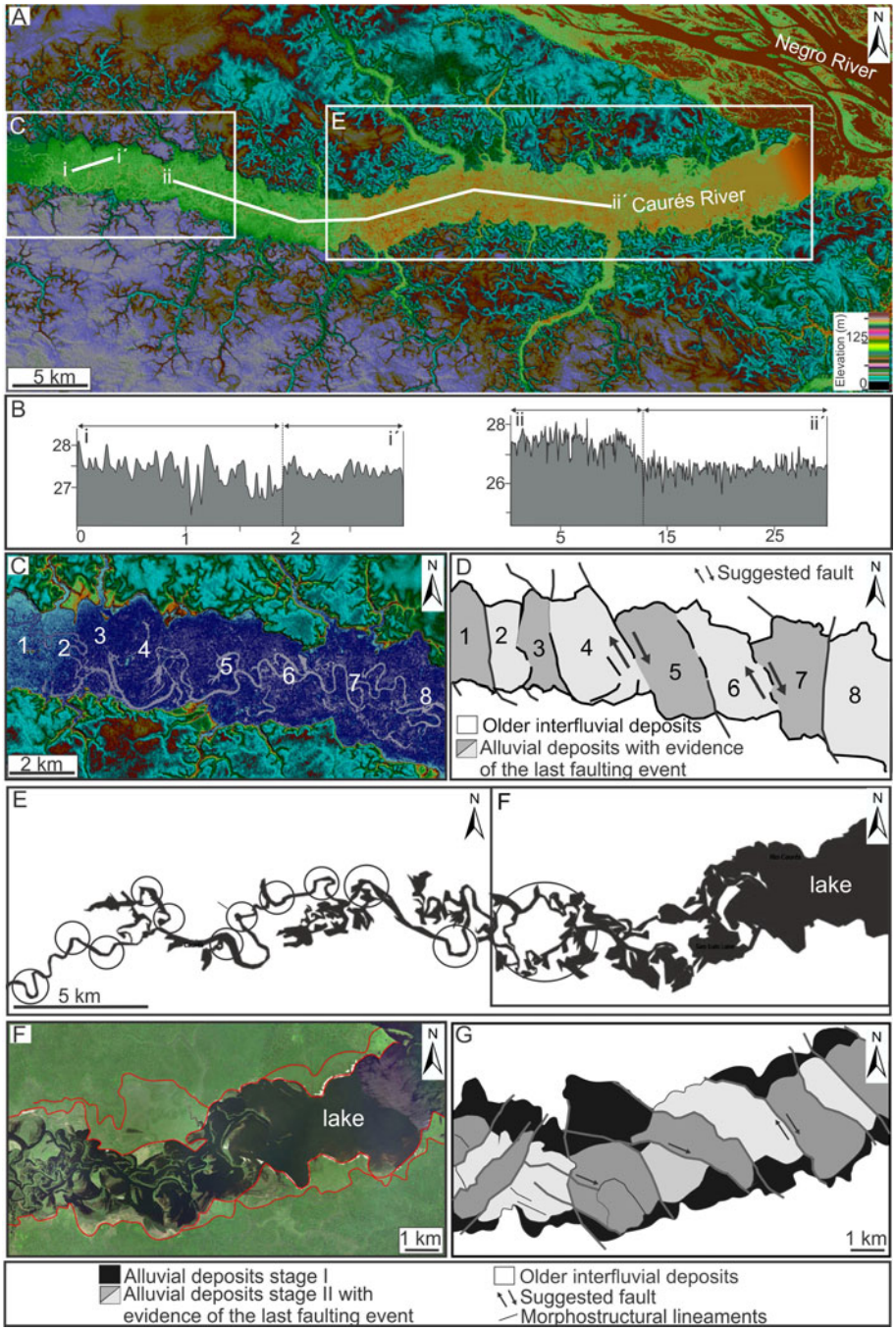

Figure 6. Morphostructural and sedimentary characteristics of the Caurés River valley. (A) General view of the valley in the radar digital elevation model (RDEM) background (see location in Figs. 2A and 4A), with locations of C and E and of the topographic transects shown in B. Note the various straight segments that form this river valley. (B) RDEM-based topographic profiles along the transects shown in A, with relief gradients detected across horizontally displaced floodplain blocks. (C and D) RDEM and corresponding drawing of various segmented floodplain blocks and changes in river courses along the valley stretch shown in A. (E) Main river valley along the stretch shown in A, characterized by frequent changes in course and local orthogonal junctions (circles). The rectangle indicates the location of F, where the river channels form a drainage pattern including a lake area that was progressively displaced downstream. (F and G) Detail of E, with sedimentary deposits of different stages marked by red lines in the Google Earth optical image of F and segmented blocks indicated in G. The darker and lighter gray colors in D and G highlight the set of en échelon-like segmented floodplain blocks. (For interpretation of the references to color in this figure legend, the reader is referred to the web version of this article.)

échelon-like lineaments (Fig. 5D–F). The latter were arranged as a series of also laterally displaced, regularly spaced floodplain blocks (Fig. 5G). The fragmented blocks most often show the opposite sense of slip, but they may also slip in the same direction (Fig. 5D).

There are parallel to near-parallel morphostructural lineaments, but their direction changes progressively through the inflection areas of the river valleys. A meandering channel having meander loops with straight sides and locally orthogonal shapes is generally in continuity with lineaments within the river valleys (Fig. 5H). Most lineaments along floodplains are NW-striking and affected floodplain deposits with dextral displacement, while NE-striking lineaments are rarer and, when present, displaced floodplain deposits sinistrally (Fig 5D).

Caurés and Unini Rivers

A succession of regularly distributed, en échelon–like floodplain blocks is also present in the Caurés (Fig. 6) and Unini (Fig. 7) river valleys. In a broad view, the lower stretch of the Caurés River valley consists of several elongated rectangular segments of floodplain deposits that change direction abruptly downstream from ESE, SE, NE, E-W, and again NE (Fig. 6A). Smooth topographic gradients of a few meters marked these inflections (Fig. 6B). Individual subdivisions of this valley are composed of many orthogonal blocks of alluvial deposits with dextral lateral displacement (Fig. 6C and D). The wide valley inflections and the morphostructural lineaments that mark the displaced floodplain blocks visibly control the development of the meandering

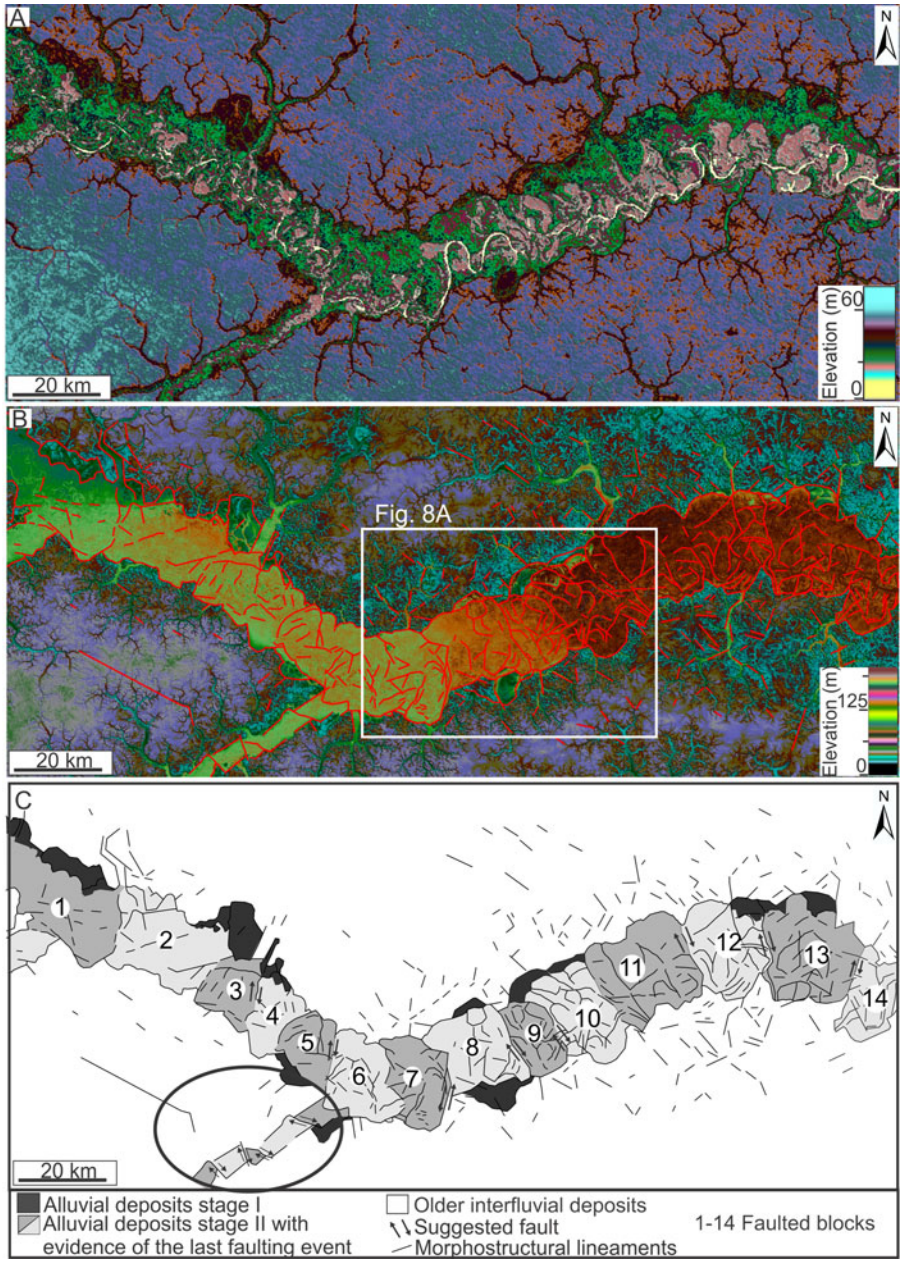

Figure 7. Morphostructural and sedimentary characteristics of the Unini River valley. (A and B) A stretch of the valley formed by straight segments with the orthogonal junction seen in the Shuttle Radar Topography Mission digital elevation model (SRTM-DEM) (A) and radar digital elevation model (RDEM) (B) (see location in Figs. 2A and 4A), with the boundary of the valley and morphostructural lineaments marked by red lines in the latter. (C) Drawing highlighting the morphostructural lineaments bounding segmented floodplain blocks detected in B. The darker and lighter gray colors in B highlight alternating en échelon-like blocks of stage II alluvial deposits. Ellipsoid = a set of dextrally displaced floodplain blocks in a tributary river. (For interpretation of the references to color in this figure legend, the reader is referred to the web version of this article.)Figure 8. (color online) Shuttle Radar Topography Mission digital elevation model (SRTM-DEM) with details of the faulted blocks. (A) Detail of Fig. 7B that illustrates a stretch of the Unini River valley where the meander loops change in shape along individual segmented floodplain blocks. (B) The faulted blocks (numbers) as indicated in Fig. 7C. (C) A stretch upstream of the same river shown in A, with a succession of horizontally displaced alluvial deposits (see the location in Fig. 4). The hatched lines indicate the boundaries of sedimentary deposits that fill the river valley.

pattern of the Caurés River (Fig. 6E), as well as the orthogonal shape of a lake formed near its confluence with the Negro River (Fig. 6E and F). In this area, both lacustrine and floodplain deposits are laterally displaced mostly by NE- and NW-striking morphostructural lineaments (Fig. 6G). The Unini River valley is narrow in its lower course, but it changes abruptly upstream into an enlarged valley as wide as 20 km, formed by long and straight segments connected orthogonally (Fig. 7A). The succession of laterally displaced blocks of floodplain deposits confined to these enlarged segments follows an orthogonal to almost orthogonal distribution with respect to the valley margins (Fig. 7B and C). Most blocks are dextrally displaced by NW- and NNE-striking lineaments and sinistrally by NE-striking lineaments (Fig. 7C). As with the Cuiuni River, most blocks slip in the opposite sense, but there is a variation in which a few blocks have the same sense of slip. Dextrally displaced floodplain blocks are recorded even in some tributaries of the Unini River (see ellipsoid in Fig. 7C). As also verified in the other studied river valleys, the meander belts in the Unini River change their shapes and sizes when crossing through displaced floodplain blocks (Fig. 8A and B). It is interesting to note that, despite similar morphostructural complexity, the Unini and Caurés river valleys have simpler depositional histories than the Cuiuni River valley. This is recorded by only two stages of floodplain deposits, with deposits of the first generation (i.e., stage I) being preserved only locally along the inner banks of the valley (Figs. 6G and 7C).

Negro River

As in the tributary valleys, both terraces of the trunk river show floodplain deposits segmented by numerous lineaments (Fig. 9A and B). In the study area, the upper and lower terraces of this river stand at SRTM elevations of 5 and 2 m above the main channel, respectively (Fig. 10A and B). These elevations align with

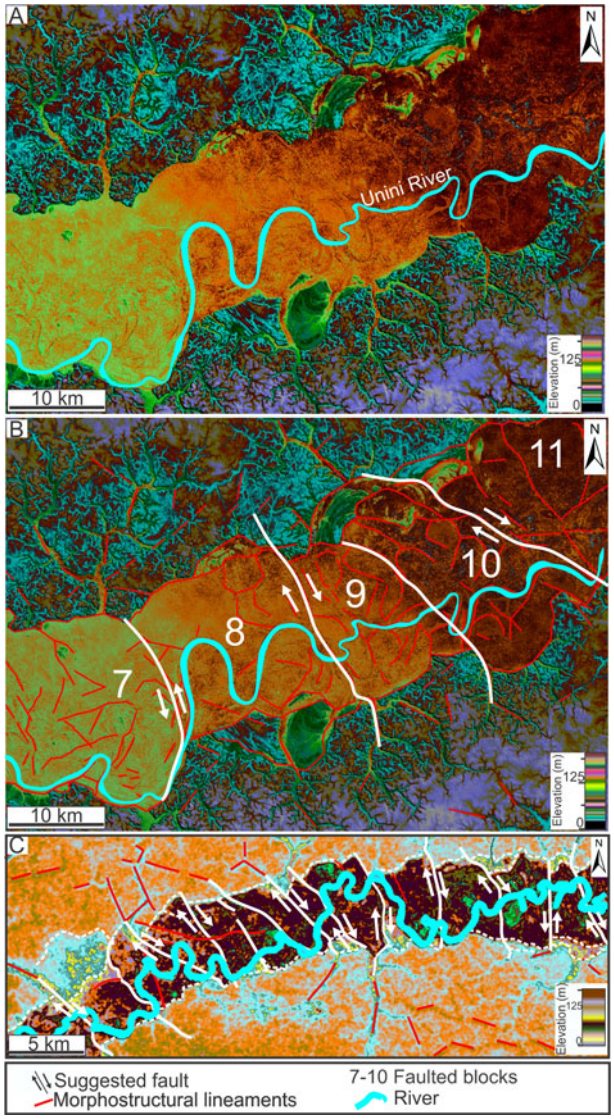

Figure 8. (color online) Shuttle Radar Topography Mission digital elevation model (SRTM-DEM) with details of the faulted blocks. (A) Detail of Fig. 7B that illustrates a stretch of the Unini River valley where the meander loops change in shape along individual segmented floodplain blocks. (B) The faulted blocks (numbers) as indicated in Fig. 7C. (C) A stretch upstream of the same river shown in A, with a succession of horizontally displaced alluvial deposits (see the location in Fig. 4). The hatched lines indicate the boundaries of sedimentary deposits that fill the river valley.

previous field observations (Latrubesse and Franzinelli, 2005). The Negro River terraces are especially extensive on the north bank of the valley, where segmented floodplain blocks are pervasive. In particular, the upper terrace, dated between >40,000 and 27,000 cal yr BP in a previous publication (Latrubesse and Franzinelli, 2005), contains several segmented blocks, many with lateral displacement. Although less extensive, segmentation continues in the lower terrace between 13,500 and 4000 cal yr BP, as also dated by those authors. Unlike the tributary valleys, which predominantly have blocks with dextral displacement, these terraces record mainly sinistrally displaced blocks (Figs. 9B and 11). Lateral offsets up to approximately 6 km are recorded (Fig. 11A), as well as topographic gradients from one block to another, measuring as low as <1 m on the L-band RDEM (Fig. 10C). Despite hindering accurate measurements, the canopy effect on the C-band SRTM-DEM highlighted the displaced blocks more efficiently (Fig. 10D), recording higher topographic contrasts due to additional vegetation changes on gradient conditions. Some secondary channels contour the displaced floodplain blocks to form a rectangular drainage pattern (Fig. 11B and C).

Magnetic data

The magnetic signature derived from the EMAG2 global model (Fig. 12A) indicates that the study area in the Solimões–Negro interfluve is dominated by two parallel positive anomalies, marked by magnetic relief with moderate amplitudes ranging from 20 to 80 nT, which contrast with adjacent areas of values below 0 to −100 nT. The morphology of the main positive anomaly is composed of two rectangular shapes, notably approximately orthogonal and aligned in WNW and NE directions to the south and north, respectively. The other anomaly, located to the southeast, is much smaller and has a general NE trend.

The shapes of the two anomalies are defined by several straight bounding lineaments. Together with several other magnetic lineaments within and external to the anomalies, these elements define a region with the structural framework characterized by a main NE trend and a subordinate NW trend (Fig. 12B).

DISCUSSION

Tectonic genesis of the morphostructural elements and deformation style

The morphological data presented herein support a tectonic control in the study area. This is suggested based on a line of evidence that includes: several long segments of tributary valleys of the Unini River, which are inflected abruptly from NE to NW, configuring orthogonal branches (Fig. 2A), added to sudden valley enlargement (Fig. 7A); the anomalously enlarged shape of the midstretch of the Negro River valley and its abrupt, nearly orthogonal downstream inflection from ENE to SE; and the lateral displacements of alluvial deposits of the Negro River terraces and also of their tributaries, the latter configuring successions of en échelon blocks, which we relate to faults. These features are similar to morphological anomalies commonly used to infer tectonic forcing in many other fluvial landforms on Earth (e.g., Miccadei et al., 2004; Jordan et al., 2005; D'Alessandro et al., 2008; Della Seta et al., 2008 and references therein; Enrico and Tommaso, 2011; Jelínek et al., 2013; Sedrette et al., 2016).

The NE- and NW-striking morphostructural lineaments paralleling the main regional structural trends of central Amazonia (e.g., Costa et al., 2001; Silva et al., 2007; Serviço Geológico do Brasil–CPRM, 2010) further support a relationship to tectonic structures. Especially, the NW-trending lineaments parallel normal and strike-slip faults that define the main course of the Negro River in the Brazilian territory (Bezerra, 2003; Franzinelli and Latrubesse, 1993; Latrubesse and Franzinelli, 2002, 2005; Rossetti 2014a, 2014b). It is interesting to recollect that this is also the trend of the strike-slip fault zone along the Purus Arch, located a few kilometers south of the Negro River valley (Fig. 13). Thus, the most likely explanation is that the NW-trending morphostructural lineaments and the half-graben of the Negro River are the result of reactivation of pre-existing structures of the Purus Arch.

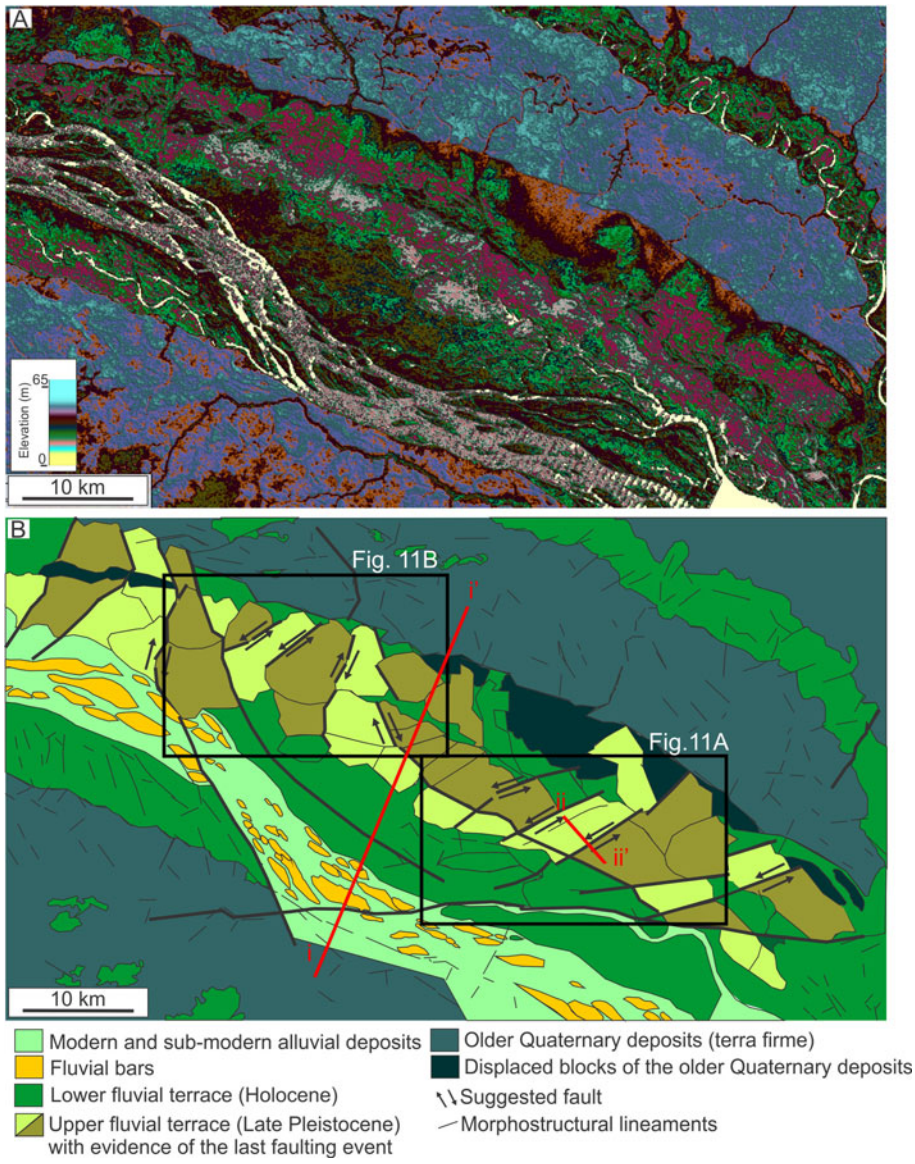

Figure 9. (color online) Morphostructural and sedimentary characteristics of the Negro River valley. (A) Shuttle Radar Topography Mission digital elevation model (SRTM-DEM) with the corresponding drawing (B) of a segment of the Negro River where fluvial terraces and modern alluvial deposits were extensively intercepted by morphostructural lineaments (see location in Figs. 2A and 4A). Note the increase in the number of lineaments, including laterally displaced ones, in the area corresponding to the upper terrace.

The NE-trending lineaments are also related to the reactivation of pre-existing structures, as these relief elements align in the same direction of main subsurface lineaments that bound the elongated sides of the rectangular-shaped magnetic anomalies. Information evidencing that these anomalies record subsurface structures is their physical continuity with the NE-trending Solimões Shear Zone that dominates the tectonic framework in the central Solimões Basin (Fig. 13). Therefore, the NE-trending morphostructural lineaments of the study area are attributed to the surface expression of deep strike-slip faults belonging to the Solimões Shear Zone. On the other hand, the NW-trending magnetic lineaments are consistent with the reactivation of NW-striking faults along the Purus Arch (see number 3 in Fig. 13), as indicated by the surface morphostructural data.

The correspondence of the NW- and NE-trending morphostructural lineaments with both the strike-slip faults of the Negro River half-graben and the deep-seated strike-slip faults of the Purus and Solimões Shear Zone leads us to propose that the relief in the study area was molded by transcurrent deformation. Testing this hypothesis might be troublesome based solely on the plan view allowed by our remote-sensing data, but some morphostructural characteristics can be used to support this interpretation. Although it is well known that faults with moderate vertical motions can produce apparent horizontal offsets, we relate the pervasive lateral offsets up to ~10 km, as verified in the study area, to fault blocks that preferentially moved laterally with no significant associated topography, typical of strike-slip faults. This interpretation is also consistent with some faults with angles ranging from 30° to 60° and the same sense of slip (e.g., Figs. 5D and 7C). However, the RDEM topographic gradients of a few meters across faulted blocks suggest local dip-slip faults, common in a strike-slip stress regime. Thus, the faulted blocks with the same sense of slip may correspond to the horizontal component of locally developed normal and, as indicated by the focal mechanism data (Fig. 3), mainly reverse faults. As such, oblique faults having normal and strike-slip components must be considered in the study area.

The prevalence of NW-striking dextral faults and NE-striking sinistral faults suggests strike-slip conjugate systems with a principal subhorizontal N-S-oriented compression and

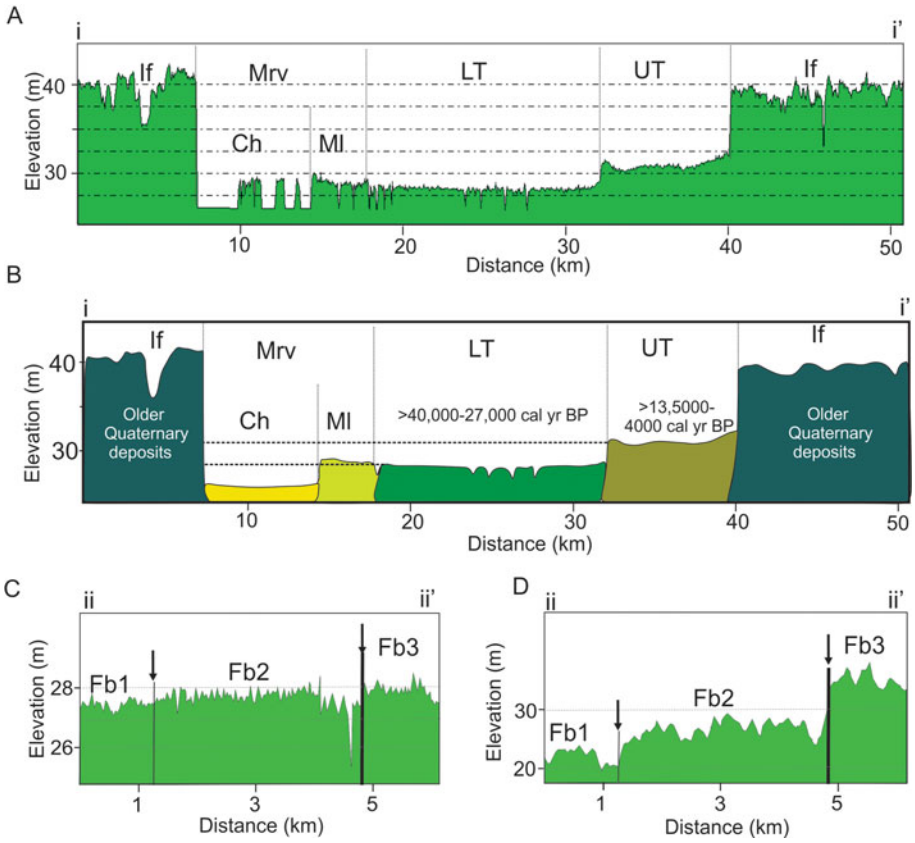

Figure 10. (color online) Topographic gradients along terraces of the Negro River. (A) Topographic profile and (B) corresponding geologic section illustrating the relief gradients transverse to the river valley. (C and D) Topographic profiles across a sinistrally displaced floodplain block based on data from Shuttle Radar Topography Mission digital elevation model (SRTM-DEM) (C) and radar digital elevation model (RDEM) (D). See Fig. 9B for the location of transects; Mrv, main river valley; Ch, main channel; Ml, marginal levee; LT, lower terrace; UT, upper terrace; If, interfluvial deposits; Fb1 to Fb3, displaced floodplain blocks. Ages shown in B are radiocarbon dating by Latrubesse and Franzinelli (2005).

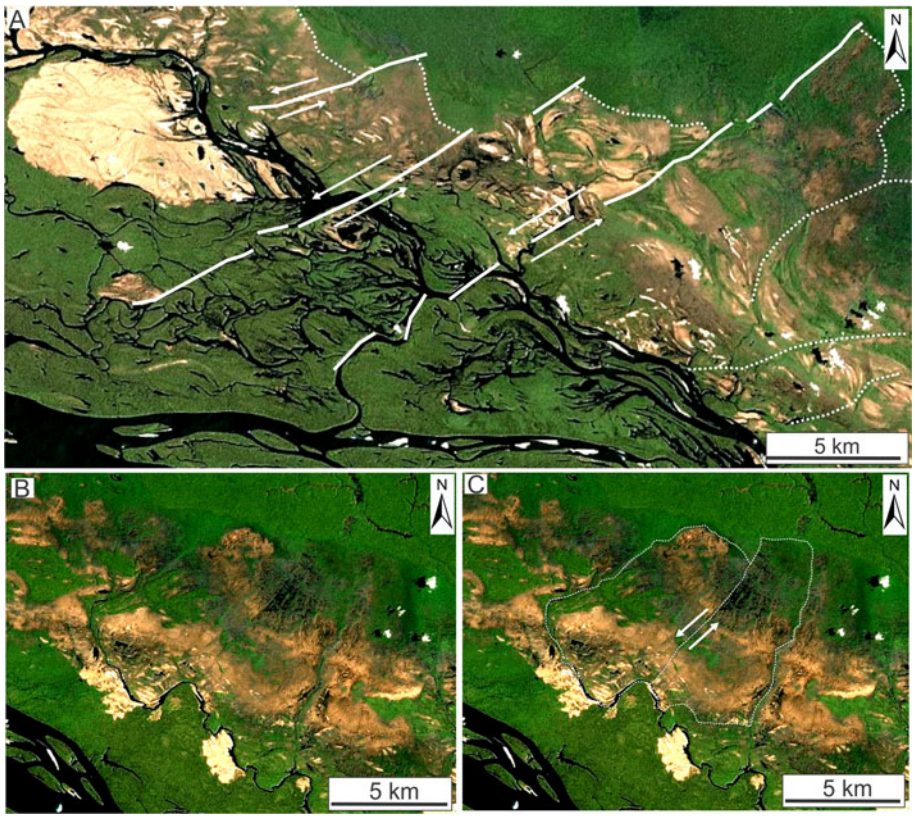

Figure 11. (color online) High-resolution optical images downloaded from WebGLEarth, with details of sinistrally displaced floodplain blocks in the Negro River valley (see location in Fig. 9B). (A) A set of three parallel, NE-striking lineaments that extend from the upper into the lower terrace/modern floodplain. (B and C) Two sinistrally displaced floodplain blocks in the upper terrace (B = C, but the latter with the structures marked; arrows indicate sense of motion along segmented blocks).

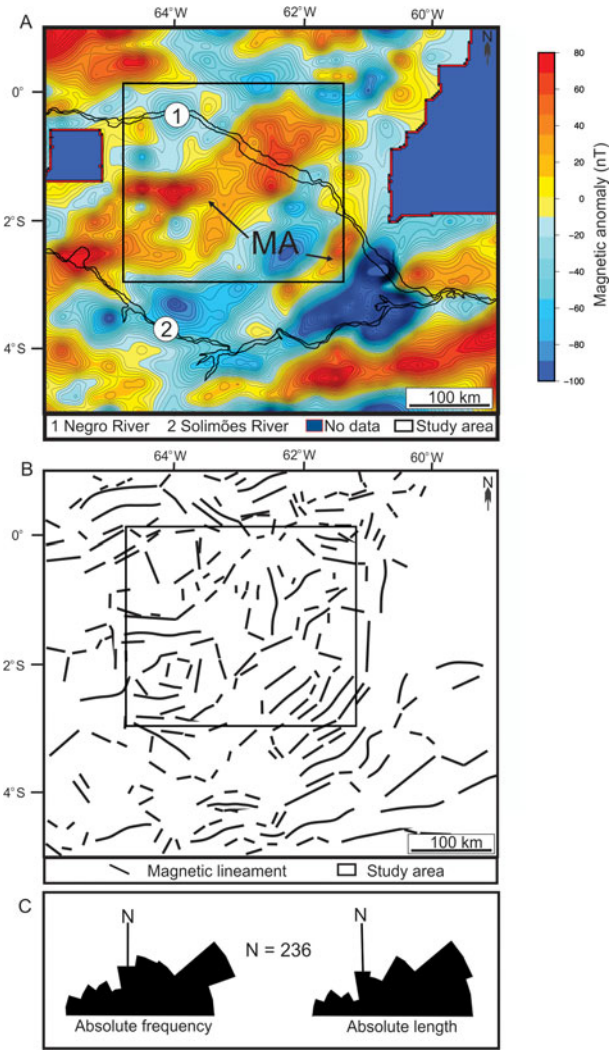

Figure 12. (color online) Subsurface data of the study area and adjacency. (A) Map with magnetic anomalies (MA = magnetic anomalies described in the text). (B) Magnetic lineaments extracted from A. (C) Rose diagrams with main modes of the magnetic lineaments shown in B. The inner boxes in A and B correspond to the study area.

E-W-oriented subhorizontal extension (Fig. 14). However, the wide range of fault strikes, particularly including the series of en échelon faults that displaced floodplain deposits along river valleys, cannot be fit in a single conjugate fault system model. One possibility is that this is due to faults that are not all coeval but record the superposition of structures generated by local stress field rotations.

Another hypothesis is that the present-day stress field reactivated pre-existing weak structures not favorably oriented for reactivation under the classical Andersonian model, as already have been described elsewhere (Sibson, 1990, 1994). Considering the conjugate model, one complication is related to the intersection angle of the faults in the study area. According to the classical theoretical Coulomb fracture criterion (e.g., Freund, 1970; Sylvester, 1988), conjugate faults usually form an acute angle around 60°. This is expected under isotropic conditions, which is not the situation in the study area. The series of en échelon faults that displaced floodplain deposits were established mostly at a high angle or even orthogonally to master faults inferred by the several NE- and NW-striking segments of the Cuiuni, Caurés, and Unini distributary river valleys (Figs. 5–8). Faults that intersect at high angles, close to normal, can be explained by the reactivation of pre-existing strike-slip and/or oblique structures. Similar faults were related to the rotation of faults initially formed at a low angle from the maximum compressive stress direction (Ramsay, 1980; Su et al., 2012).

Estimating the deformation chronology

Establishing when the stress fields were reactivated in the study area is troublesome. Even though the described structures are all found on sedimentary deposits mapped mostly as Quaternary in age, one cannot fully discard the hypothesis of their inheritance from long-inactive past tectonic geometries. However, this hypothesis would require a Quaternary cover thin enough to reveal the underlying structures. Although the thickness of the studied deposits may vary from one place to another due to fluvial erosion, it would be expected that the average thickness known for this unit (80 m cf. Maia et al., 1977; Reis et al., 2006) would have been sufficient to cover the signs of long-inactive pre-existing structures.

Therefore, a plausible explanation is that failure occurred due to the reactivation of pre-existing structures sometime in the late Pleistocene and even late Holocene, in line with our data. This proposed time for the tectonic activity is consistent with fault displacement in the deposits of the upper and lower terraces of the trunk river, with ages between >40,000 and 27,220 ± 200 yr BP and between 13,420 ± 100 and 4050 ± 50 yr BP, respectively (cf. Latrubesse and Franzinelli, 2005). The fact that the upper terrace shows a higher concentration of faults relative to the lower terrace may evidence a more intense event before the formation of the lower terrace, that is, sometime before 13,000 yr BP in the late Pleistocene.

Active tectonics also displaced the alluvial deposits of many tributaries of the Negro River valleys, as indicated by: the orthogonal shape of displaced deposits, defined by straight lineaments; the continuity of many of these bounding lineaments into older interfluvial Quaternary deposits; and the successions of rectangular blocks laterally arranged in an en échelon pattern, which are related to fissures and faults that laterally displaced the latest deposits formed within the valleys.

The multistory river valley fills suggest multiple tectonic events within the late Pleistocene–Holocene, and probably also the continuity of the deformation even in the present day. In particular, the floodplain deposits displaced by faults in the Cuiuni River valley (Fig. 5) indicate at least four stages of valley fill, each resulting in fragmented, rectangular-shaped deposits that were often horizontally displaced by strike-slip faults. Although the Caurés and Unini river valleys document only two stages of floodplain deposits (Figs. 6–8), the pervasive fracturing evidenced by the sets of horizontally displaced rectangular blocks, following a pattern similar to the stage IV deposits of the Cuiuni River valley, may be related to active tectonics postdating even the last depositional event. The rectangular shape of rivers with orthogonal junctions that continues into fractures and fault planes in these tributary rivers (e.g., Figs. 5G and H and 6C) and the changes in the shape and size of meander belts when crossing individual faulted blocks (Fig. 8A and B) are additional characteristics compatible with present-day active tectonics. This interpretation is also consistent with the orthogonal shape of the lake in the lower Caurés River near the confluence with the Negro River, which follows the

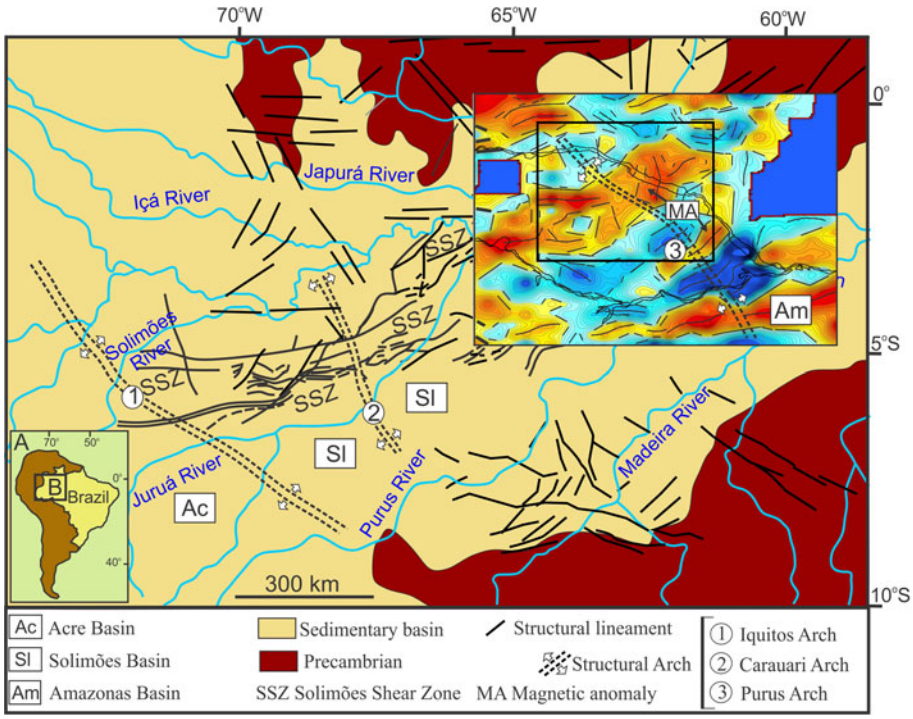

Figure 13. (color online) Magnetic map overlapped on a simplified geologic map to show the continuity of NE-trending anomalies with the Solimões Shear Zone. The box inserted in the magnetic map locates the study area.

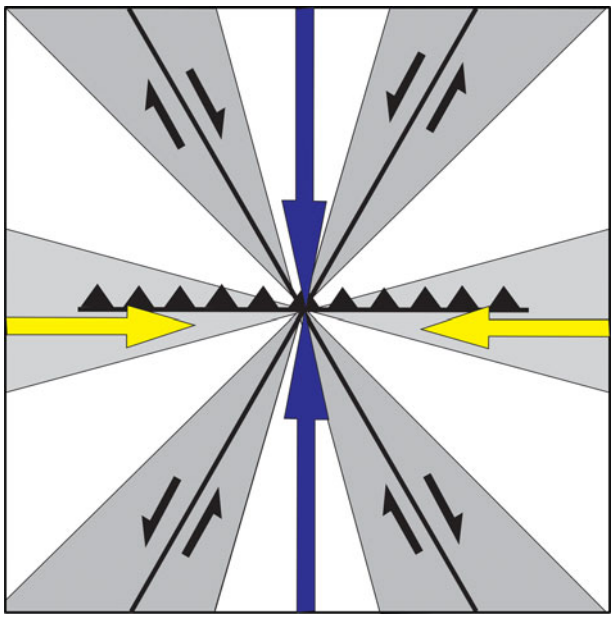

Figure 14. Regional structural schematic model with the stress fields proposed for the study area. The region is under a N-S-oriented subhorizontal maximum compression (σ1, blue arrows) and an E-W-oriented subhorizontal minimum compression (σ3, yellow arrows); the intermediate stress (σ2) is vertical. The model shows conjugate faults (black lines) consisting of dextral NW-SE strike-slip and sinistral NE-SW strike-slip faults. The gray area corresponds to the range of directions of lineaments observed in the study area. (For interpretation of the references to color in this figure legend, the reader is referred to the web version of this article.)

Table 1. List of main earthquakes recorded in Amazonian states since 2005.

Year	Magnitude (Richter scale)	Main location (State)
2005	5.0	Mato Grosso
2007	6.1	Amazonas, Acre
2010	4.9	Amazonas, Acre
2010	3.5, 2.3, 2.4	Mato Grosso
2010	4.9	Amazonas
2010	4.7, 6.5	Acre
2010	5.0	Tocantins
2011	7.0	Acre, Amazonas
2012	7.1	Amazonas
2013	5.2	Acre
2014	5.1	Acre
2015	3.1, 4.1	Acre, Mato Grosso
2015	7.6	Acre, Rondônia, Amazonas
2015	4.9, 4.6, 5.1, 6.7	Acre
2016	4.0	Amazonas
2017	6.1	Amazonas
2018	7.3	Acre, Amapá, Amazonas, Pará, Roraima
2019	6.8	Acre

Source: https://pt.wikipedia.org/wiki/Lista_de_sismos_no_Brasil (accessed February 10, 2020).

same pattern of strike-slip faults with dextral motion recorded upstream in this valley (Fig. 6G).

The hypothesis of present-day or near-present-day active tectonics in central Amazonia is compatible with: (1) the local but intense compartmentalization of forest habitats and pervasive tree mortality only a few tens of centuries ago in a wetland confined to a tectonic depression (Rossetti et al. (2019); (2) the tectonic subsidence <2000 cal yr BP of an area of the central

Viruá megafan (Rossetti et al., 2017b); (3) the seismite in terrace deposits at the margin of the Madeira River, dated at 1382–1341 cal yr BP and related to an earthquake of a magnitude of at least 6 on the Richter scale (Rossetti et al., 2017a); and (4) the several records of fault reactivation controlling Amazonian river systems (e.g., Franzinelli et al., 1999; Bezerra, 2003; Costa et al., 2001; Latrubesse and Franzinelli, 2005; Almeida-Filho and Miranda, 2007; Soares, 2007; Hayakawa et al., 2010; Val et al., 2013; Ibanez et al., 2014).

Although in situ measurements of seismological events are still scarce in Brazilian Amazonia, the available data are compatible with the proposed present-day tectonic activity. The first seismological report was made by a missionary in 1692, who described severe environmental damage (see descriptions in IHGB, 1917) close to the mouth of the Negro River, later related to an earthquake of magnitude up to 7.0 (Veloso, 2014) on the Richter scale. In addition, earthquakes of magnitudes 5.1 and 5.5 that affected the left bank of the Negro river in 1963 and 1983 (Assumpção et al., 1983) were related to NW-striking maximum horizontal compressive stresses (Assumpção and Suárez, 1988). The seismological record in the Amazonian region has expanded in recent years (e.g., Assumpção et al., 2014); Table 1 lists the main events since 2005. Although some of these events occurred at great depths (i.e., even hundreds of kilometers), earthquake hypocenters only a few kilometers deep have also been recorded. Much further work, including breakout data and in situ measurements, is still needed to establish the causes of these Amazonian earthquakes, but a direct relationship with fault reactivation has been demonstrated in some cases (e.g., Santos et al., 2019).

Late-stage stress field in intraplate South America

The principal subhorizontal N-S-oriented compression and E-W-oriented horizontal extension toward the intraplate Amazonian basin distinct from the overall ~E-W pattern seen in most areas of the South American plate was already in effect since at least the late Pleistocene–Holocene. Mantle convection-driven dynamic topography has been generally indicated as a main source of intraplate stresses (Müller et al., 2000) or hot spots (Brodie and White, 1994). This mechanism has been claimed as the source of deformation in central Amazonia in the Miocene (Shepard et al., 2010) and the middle and late Pleistocene (Val et al., 2013).

Mantle convection has long been known to drive plate tectonics (e.g., Holmes, 1931; Coltice et al., 2017); thus, the neotectonic stresses within the South American plate might be a result of the continued westward plate motion that caused the breakup of the Farallon plate into the Cocos and Nazca plates in the opposite side, where the latter is subducting (Tebbens and Cande, 1997). It follows that central Amazonia, located in a complex intraplate region under the influence of these two stress fields, is expected to be an area of great neotectonic instability also caused by plate motion (Ojeda and Whitman, 2002; Pérez-Gussinyé et al., 2007).

Plate displacement since the Miocene had consequences on driving forces in the Andes and likely producing intraplate stresses (Jaillard et al., 2000; Garzione et al., 2008; Assumpção et al., 2016). For instance, intraplate tectonics by W-E compression in the Andes during the Pliocene–Pleistocene (Mercier et al., 1992; Coudert et al., 1995) reactivated strike-slip faults and produced a shallow (i.e., <500-m-thick) but broad subsiding basin in central Brazil known as the Pantanal Matogrossense wetlands (Catto, 1975). In addition, since the Miocene, episodes of Andean uplift coeval with major plate shifts caused uplift and basin inversion in northeastern Brazil (e.g., Bezerra and Vita-Finzi, 2000; Pedoja et al., 2011; Rossetti et al., 2013; Gandini et al., 2014; Alves et al., 2019; Bezerra et al., 2008, 2014, 2020). These changes were related to the rotation from the Late Cretaceous N-S maximum compressive stress field to the E-W and, secondarily, NW-SE stress fields from the middle Miocene to the present (Bezerra et al., 2020).

The focal mechanism showing NE- and NW-striking strike-slip and dip-slip faults recorded in the study area during the late Pleistocene–Holocene is compatible with that prevailing regionally during the evolution of the Solimões Basin (Caputo and Soares, 2016). The continuity of the NE-striking faults of central Amazonia beyond the Brazilian border, for instance, into the Peruvian and Bolivian foreland basins at the boundary between the sub-Andes and the Brazilian Craton (Dumont, 1996), sustains a relationship with the tectonic dynamics of the South American plate, as these structures parallel the principal regional stress fields theorized for this plate.

Although the stress field in the study area might be in part attributed to the interplay of plate motion and Andean rise, the deformation style was slightly different compared with the prevailing E-W maximum horizontal stresses of areas located at the plate margin and in the sub-Andean region, as well as throughout most of western South America (Assumpção, 1992; Riccomini and Asumpção, 1999; Assumpção et al., 2016; Heidbach et al., 2018). The variation of the present-day maximum compressive stress field from E-W to NW-SE toward central Amazonia indicated by numerical models (Fig. 3) and the late Pleistocene–Holocene principal subhorizontal N-S-oriented compression recorded in the present work lead us to argue also for the contribution of local stresses, to be determined in future investigations.

CONCLUSIONS

We conclude that the present-day relief of the study area in central Amazonia has a geologically recent tectono-sedimentary history that spans the late Pleistocene and Holocene. During this interval, fluvial valleys in the Negro River basin were filled by sediments through multiple depositional episodes. The integration of relief elements with subsurface geologic and geophysical data led us to relate NE- and NW-trending morphostructural lineaments to the reactivation of pre-existing strike-slip faults. Fault Reactivation may explain the wide range of strike directions and the high angle of intersection of the observed faults. These features may also be explained under a conjugate strike-slip regime, as suggested by the main NE- and NW-striking strike-slip faults, respectively with sinistral and dextral motions, and the oblique (normal and reverse) faults. The conjugate systems would record deformation under N-S-oriented horizontal compression and E-W-oriented horizontal extension. While the assessment of structures unequivocally related to faults has been previously documented using remote sensing, the main significance of the present work is that it is the first to record fluvial deposits with extensive faulting, including an abundance of laterally distributed strike-slip faults, over a large area of the Negro River basin. Although these episodes of tectonic deformation were in part imposed by the interplay of plate motion and Andean uplifting since the late Pleistocene, additional local factors that remain to be determined probably also contributed.

Acknowledgments. The Brazilian National Council for Scientific and Technological Development-CNPq is acknowledged for providing research fellowships to DFR and FHRB. SIPAM provided the radar RDEM. We thank the two reviewers, Frank Audemard and Siddartha Kumar Lahiri, whose comments and suggestions helped to significantly improve an early version of the article. We also wish to acknowledge the support offered by associate editor J. Urrutia Fucugauchi and senior editor Nicholas Lancaster, who provided constructive corrections and comments during the review process.

REFERENCES

Almeida-Filho, R., Miranda, F.P., 2007. Mega capture of the Rio Negro and formation of the Anavilhanas Archipelago, Central Amazonia, Brazil: evidences in SRTM digital elevation model. *Remote Sensing of Environment* **110**, 387–392.

Alves, F.C., Rossetti, D.F., Valeriano, M.M., Andrades Filho, C.O., 2019. Neotectonics in the South American passive margin: evidence of Late Quaternary uplifting in the northern Paraíba Basin (NE Brazil). *Geomorphology* **325**, 1–16.

Assumpção, M., 1992. The regional intraplate stress field in South America. *Journal of Geophysical Research Solid Earth* **97**, 11889–11903.

Assumpção, M., Dias F.L., Zevallos, I., Naliboff, J., 2016. Intraplate stress field in South America from earthquake focal mechanisms. *Journal of South American Earth Sciences* **71**, 278–295.

Assumpção, M., Ferreira, J., Barros, L., Bezerra, F.H.R., Fraça, G.S., Barbosa, J.R., Menezes, E., *et al.*., 2014. In: Talwani, P. (Ed.), *Intraplate Earthquakes*. Vol. 1. Cambridge University Press, Cambridge, pp. 50–71.

Assumpção, M., Ortega, R., Berrocal, J., Veloso, J.A.V., 1983. O sismo de Codajás-AM, de 05.08.1983. *Revista Brasileira de Geofísica* **2**, 39–44.

Assumpção, M., Suárez, G., 1988. Source mechanisms of moderate-size earthquakes and stress orientation in mid-plate South America. *Geophysical Journal* **9**, 253–267.

Assumpção, M., Suarez, G., Veloso, J.A., 1985. Fault plane solutions of intraplate earthquakes in Brazil: some constraints on the regional stress field. *Tectonophysics* **113**, 283–293.

Barros, L.V., Assumpção, M., Quintero, R., Caixeta, D., 2009. The intraplate Porto dos Gaúcos seismic zone in the Amazon craton. *Tectonophysics* **469**, 37–47.

Bezerra, F.H., Castro, D.L., Maia, R.P., Sousa, M.O.L., Moura-Lima, E.N., Rossetti, D.F., Bertotti, G., Souza, Z.S., Nogueira, F.C.C., 2020. Postrift stress field inversion—implications for the petroleum system in the Potiguar Basin and evolution of the equatorial margin of South America. *Journal of Marine and Petroleum Geology* **111**, 88–104.

Bezerra, F.H.R., Brito Neves, B.B., Correa, A.C.B., Barreto, A.M.F., Suguio, K., 2008. Late Pleistocene tectonic-geomorphological development within a passive margin—the Cariatá trough, northeastern Brazil. *Geomorphology* **97**, 555–582.

Bezerra, F.H.R., Rossetti, D.F., Oliveira, R.G., Brito Neves, B.B., Medeiros, W.E., Balsamo, F., Nogueira, F.C., Dantas, E.L., Góes, A.M., Andrades Filho, C.O., 2014. Neotectonic fault reactivation of basement fabric controls sediment deposition and deformation in the continental margin of NE Brazil. *Tectonophysics* **614**, 78–90.

Bezerra, F.H.R., Vita-Finzi, C. 2000. How active is a passive margin? Paleoseismicity in northeastern Brazil. *Geology* **28**, 591–594.

Bezerra, P.E.L., 2003. *Compartimentação morfotectônica do interflúvio Solimões-Negro*. Ph.D. thesis, Universidade Federal do Pará, Belém, Pará, Brazil.

Bosworth, W., 2008. North Africa–Mediterranean present-day stress field transition and implications for fractured reservoir production in the eastern Libyan basins. *Geology of East Libya* **4**, 123–138.

Braiais, J., Guillocheau, F., Lasseur, E., Robin, C., Châteauneauf, J.J., Serrano, O., 2016. Response of low-subsiding intracratonic basin to long wavelength deformations: the Palaeocene–early Eocene period in the Paris Basin. *Solid Earth* **7**, 205–228.

Braitenberg, C., Ebbing, J., 2009. The GRACE-satellite gravity and geoid fields in analysing large-scale cratonic or intracratonic basins. *Geophysical Prospecting* **57**, 559–571.

Brodie, J., White, N.J., 1994. Sedimentary basin inversion caused by igneous underplating: northwest European continental shelf. *Geology* **22**, 147–150.

Caputo, M.V., Soares, E.A.A., 2016. Eustatic and tectonic change effects in the reversion of the transcontinental Amazon River drainage system. *Brazilian Journal of Geology* **46**, 301–328.

Catto, A.J., 1975. *Análise Geológica e Geofísica da Bacia do Pantanal Matogrossense*. Internal Report. Petrobras, Rio de Janeiro.

Ciardelli, C., Assumpção, M., 2019. Rupture lengths of intraplate earthquakes in Brazil determined by relative location of aftershocks: evidence for depth dependence of stress drops. *Journal of South American Earth Sciences* **89**, 246–258.

Coltice, N., Gérault, M., Ulvrová, M., 2017. A mantle convection perspective on global tectonics. *Earth-Science Reviews* **165**, 120–150.

Costa, J.B.S.C., Bemerguy, R.L., Hasui, Y., Borges, M.S., 2001. Tectonics and paleogeography along the Amazon River. *Journal of South American Earth Sciences* **14**, 335–347.

Coudert, L., M., Frappa, C., Viguier, C., Arias, C., 1995. Tectonic subsidence and crustal flexure in the Neogene Chaco basin of Bolivia. *Tectonophysics* **243**, 277–292.

D'Alessandro, L., Miccadei, E., Piacentini, T., 2008. Morphotectonic study of the lower Sangro River valley (Abruzzi, central Italy). *Geomorphology* **102**, 145–158.

Della Seta, M., Monte, M., Fredi, P., Miccadei, E., Nesci, O., Pambianchi, G., Piacentini, T., Troiani, F., 2008. Morphotectonic evolution of the Adriatic piedmont of the Apennines: an advancement in the knowledge of the Marche-Abruzzo border area. *Geomorphology* **102**, 119–129.

Doré, A.G., Lundin, E.R., Kusznir, N.J., Pascal, C., 2008. Potential mechanisms for the genesis of Cenozoic domal structures on the NE Atlantic margin: pros, cons and some new ideas. In: Johnson, H., Doré, A.G., Gatliff, R.W., Holdsworth, R.E, Lundin, R., Ritchie, J.D. (Eds.), *The Nature and Origin of Compression in Passive Margins. Geological Society Special Publication* 306, 1–26.

Dumont, J.F., 1996. Neotectonics of the Subandes-Brazilian craton boundary using geomorphological data: the Marañon and Beni basins. *Tectonophysics* **259**, 137–151.

Enrico, M., Tommaso, P., 2011. Two tectonic geomorphology studies on the landscape and drainage network of chain and piedmont areas of the Abruzzi region (central Apennines, Italy). In: Schattner, U. (Ed.), *New Frontiers in Tectonic Research—At the Midst of Plate Convergence*. IntechOpen, Rijeka, Croatia, pp. 173–214.

Franzinelli, E., Igreja, H., 2002. Modern sedimentation in the lower Negro River, Amazonas State, Brazil. *Geomorphology* **44**, 259–271.

Franzinelli, E., Igreja, H., Repolho, T. 1999. Fragmentation of ecosystem owing to neotectonics in the Amazon basin. *Science Reports of Tohoku University*, 7th series 49, 207–214.

Franzinelli, E., Latrubesse, E., 1993. Neotectonic in the central part of the Amazon basin. *Bulletin of the INQUA Neotectonic Commission* **16**, 10–13.

Freund, R., 1970. Rotation of strike-slip faults in Sistan, southeast Iran. *Journal of Geology* **78**, 188–200.

Gandini, R., Rossetti, D.F., Netto, R., Bezerra, F.H.R., Góes, A.M., 2014. Neotectonic evolution of the Brazilian northeastern continental margin based on sedimentary facies and ichnology. *Quaternary Research* **82**, 462–472.

Garzione, C.N., Hoke, G.D., Libarkin, J.C., Withers, S., MacFadden, B., Eiler, J., Ghosh, P., Mulch, A., 2008. Rise of the Andes. *Science* **320**, 1304–1307.

Gunnell, Y., Fleitout, L., 2000. Shoulder uplift of the Western Ghats passive margin, India: a denudational model. *Earth Surface Processes and Landforms* **23**, 391–404.

Hayakawa, E.H., Rossetti, D.F., Valeriano, M.M., 2010. Applying DEM–SRTM for reconstructing a late Quaternary paleodrainage in Amazonia. *Earth and Planetary Science Letters* **297**, 262–270.

Heidbach, O., Rajabi, M., Cui, X., Fuchs, K., Müller, B., Reinecker, J., Reiter, M., *et al.*., 2018. The World Stress Map database release 2016: crustal stress pattern across scales. *Tectonophysics* **744**, 484–498.

Holmes, A., 1931. Radioactivity and earth movements. *Transactions of the Geological Society of Glasgow* **18**, 559–606.

Holmes, A., 1965. *Principles of Physical Geology*. 2nd ed. Thomas Nelson, London.

Howard, A.D., 1967. Drainage analysis in geologic interpretation: a summation. *American Association of Petroleum Geologists Bulletin* **51**, 2246–2259.

Hudec, M., Jackson, M.P.A., 2002. Structural segmentation, inversion, and salt tectonics on a passive margin: evolution of the Inner Kwanza Basin, Angola. *Geological Society of America Bulletin* **115**, 639–640.

Ibanez, D.M., Riccomini, C., Miranda, F.P., 2014. Geomorphological evidence of recent tilting in the Central Amazonia region. *Geomorphology* **214**, 378–387.

IHGB, 1917. O Diário do Padre Samuel Fritz. *Revista do Instituto Histórico e Geográfico Brasileiro* **81**, 354–397.

Instituto Nacional de Pesquisas Espaciais–INPE, 2008. Topodata: banco de dados geomorfométricos do Brasil. http://www.dsr.inpe.br/topodata/data/geotiff (accessed on January 11th, 2021).

Jaillard, E., Hérail, G., Monfret, T., Díaz–Martínez, E., Baby, P., Lavenu, A., Dumont, J.F., 2000. Tectonic evolution of the Andes of Ecuador, Peru, Bolivia and northernmost Chile. In: Cordani, U.G., Milani, E.J., Thomaz Filho, A., Campos, D.A. (Ed.), *Tectonic Evolution of South America*. 31st International Geological Congress, Rio de Janeiro, Brazil, pp. 481–559.

Jelínek, J., Stanek, F., Thomas, J., Danek, T., Malis, J., 2013. The application of morphostructural analysis and its validation by comparison with documented faults within the Zlaté Hory ore district (the northeastern part of the Bohemian massif). *Acta Geodynamic et Geomaterialia* **10**, 5–17.

Jordan, G., Meijninger, B.M.L., van Hinsbergen, D.J.J., Meulenkamp, J.E., van Dijk, P.M., 2005. Extraction of morphotectonic features from DEMs: development and application for study areas in Hungary and NW Greece. *International Journal of Applied Earth Observation and Geoinformation* **7**, 163–182.

Kellndorfer, J.W., Pierce, L., Dobson, C., Fites, J.A., Hunsaker, C., Vona, J., Clutter, M., 2004. Vegetation height estimation from Shuttle Radar Topography Mission and National Elevation Datasets. *Remote Sensing of Environment* **3**, 339–258.

Latrubesse, E.M., Cozzuol, M., Silva-Caminha, S.A.F., Rigsby, C.A., Absy, M.L., Jaramillo, C.A., 2010. The Late Miocene paleogeography of the Amazon Basin and the evolution of the Amazon River system. *Earth-Science Reviews* **99**, 99–124.

Latrubesse, E.M., Franzinelli, E., 2002. The Holocene alluvial plain of the middle Amazon River, Brazil. *Geomorphology* **44**, 241–257.

Latrubesse, E.M., Franzinelli, E., 2005. The late Quaternary evolution of the Negro River, Amazon, Brazil: implications for island and floodplain formation in large anabranching tropical systems. *Geomorphology* **70**, 372–397.

Maia, R.G., Godoy, H.K., Yamaguti, H.S., Moura, P.A., Costa, F.S., 1977. *Projeto carvão no Alto Amazonas*. CPRM, Rio de Janeiro.

Maurin, J.C., Guiraud, R., 1993. Basement control in the development of the early cretaceous West and Central African rift system. *Tectonophysics* **228**, 81–95.

Maus, S., Barckhausen, U., Berkenbosch, H., Bournas, N., Brozena, J., Childers, V., Dostaler, F., *et al.*., 2009. EMAG2: a 2–arc min resolution Earth Magnetic Anomaly Grid compiled from satellite, airborne, and marine magnetic measurements. *Geochemistry, Geophysics, Geosystems* **10** (8), Q08005.

Mercier, J.L., Sebrier, M., Lavenu, A., Cabrera, J., Dumont, O., Machare, J., 1992. Changes in the tectonic regime above a subduction zone of Andean-type: the Andes of Peru and Bolivia during the Pliocene–Pleistocene. *Journal of Geophysical Research* **97**, 11945–11982.

Miccadei, E, Paron, P., Piacentini, T., 2004. The SW escarpment of the Montagna del Morrone (Abruzzi, central Italy): geomorphology of a faulted-generated mountain front. *Supplementi di Geografia Fisica e Dinamica Quaternaria* **27**, 55–87.

Moulin, M., Aslanian, D., Unternehr, P., 2010. A new starting point for the South and Equatorial Atlantic Ocean. *Earth-Science Reviews* **98**, 1–37.

Müller, R.D., Lim, V.S.L., Isern, A.R., 2000. Late Tertiary tectonic subsidence on the northeast Australian passive margin: response to dynamic topography? *Marine Geology* **162**, 337–352.

Ojeda, G.Y., Whitman, D., 2002. Effect of windowing on lithosphere elastic thickness estimates obtained via the coherence method: results from northern South America. *Journal of Geophysical Research* **107**, ETG 3–1–ETG 3–12.

Pedoja, K., Husson, L., Regard, V., Cobbold, P.R., Ostanciaux, E., Johnson, M.E., Kershaw, S., *et al.*., 2011. Relative sea–level fall since the last interglacial stage: are coasts uplifting worldwide? *Earth-Science Reviews* **108**, 1–15.

Pérez-Gussinyé, M., Lowry, A.R., Watts, A.B., 2007. Effective elastic thickness of South America and its implication for intracontinental deformation. *Geochemistry, Geophysics, Geosystems* **8**, Q05009.

Polidori, L., Simonetto, E., 2014. Effect of scale on the correlation between topography and canopy elevations in an airborne InSAR product over Amazonia. *Procedia Technology* **16**, 180–185.

Ramsay, J., 1980, Shear zone geometry: a review. *Journal of Structural Geology* **2**, 83–99.

Reis, N.J., Almeida, M.E., Riker, S.L., Ferreira, A.L., 2006. Geologia e Recursos Minerais do Estado do Amazonas: sistema de informações geográficas–SIG: texto explicativo do mapa geológico e de recursos minerais do Estado do Amazonas. Escala 1.1:000.000. Mapas Geológicos Estaduais, Programa Geologia do Brasil, CPRM, Manaus.

Riccomini, C., Assumpção, M., 1999. Quaternary tectonics in Brazil. *Episodes* **22**, 221–225.

Rosa, J.W.C., Rosa, J.W.C., Fuck, R.A., 2014. Geophysical structures and tectonic evolution of the southern Guyana shield, Brazil. *Journal of South American Earth Sciences* **52**, 57–71.

Rossetti, D.F., 2014a. Imaging underwater neotectonic structures in the Amazonian lowland. *The Holocene* **24**, 1269–1277.

Rossetti, D.F., 2014b. The role of tectonics in the late Quaternary evolution of Brazil's Amazonian landscape. *Earth-Science Reviews* **139**, 362–389.

Rossetti, D.F., Alves, F.C., Valeriano, M.M., 2017a. A tectonically-triggered late Holocene seismite in the southern Amazonian lowlands, Brazil. *Sedimentary Geology* **358**, 70–83.

Rossetti, D.F., Bezerra, F.H.R., Dominguez, J.M.L., 2013. Late Oligocene–Miocene transgressions along the equatorial and eastern margins of Brazil. *Earth-Science Reviews* **123**, 87–112.

Rossetti, D.F., Molina, E. C. Cremon, E.H., 2016. Genesis of the largest Amazonian wetland in northern Brazil inferred by morphology and gravity anomalies. *Journal of South American Earth Sciences* **69**, 1–10.

Rossetti, D.F., Toledo, P.M., Góes, A.M., 2005. New geological framework for western Amazonia (Brazil) and implications for biogeography and evolution. *Quaternary Research* **63**, 78–89.

Rossetti, D.F., Toledo, P.M., Valeriano, M.M., 2019. Neotectonics and tree mortality in a forest ecosystem of the Negro basin: geomorphic evidence of contemporary seismicity in the intracratonic Brazilian Amazonia. *Geomorphology* **329**, 138–151.

Rossetti, D.F., Valeriano, M.M., Gribel, R., Cohen, M.C.L., Tatumi, S.H., Yee, M. 2017b. The imprint of Late Holocene tectonic reactivation on a megafan landscape in the northern Amazonian wetlands. *Geomorphology* **295**, 406–418.

Santos, W.L., Crisóstomo, C.A., Barbosa, A.R.F., Silva, P.M., Nascimento, F.I.C., 2019. Atividades sísmicas na Amazônia: levantamento e caracterização de terremotos na Amazõnia sul-ocidental, Acre, Brasil. *Revista GeoUECE* **8**, 66–77.

Sedrette, S., Rebai, N., Mastere, M., 2016. Evaluation of neotectonic signature using morphometric indicators: case study in Nefza, northwest of Tunisia. *Journal of Geographic Information System* **8**, 338–350.

Serviço Geológico do Brasil–CPRM, 2010. Mapa geológico do Brasil (accessed December 2010). http://geobank.sa.cprm.gov.br.

Shepard, G.E., Müller, R.D., Gurnis, M., 2010. Miocene drainage reversal of the Amazon River driven by plate-mantle interaction. *Nature Geoscience* **3**, 870–875.

Sibson, R.H., 1990. Conditions for fault-valve behaviour. In: Knipe, R.J., Rutter, E.H. (Eds.), *Deformation Mechanisms, Rheology and Tectonics. Geological Society of London Special Publication* 54, 15–28.

Sibson, R.H., 1994. An assessment of field evidence for Byerlee friction. *Pure and Applied Geophysics* **142**, 645–662.

Silva, C.L., Morales, N., Crósta, A.P., Costa, S.S., Jiménez-Rueda, J.R., 2007. Analysis of tectonically-controlled fluvial morphology and sedimentary processes of the western Amazon basin: an approach using satellite images and digital elevation model. *Anais da Academia Brasileira de Ciências* **79**, 693–711.

Soares, E.A.A., 2007. *Depósitos Pleistocenos da Região de Confluência dos Rios Negro e Solimões, Porção Oeste da Bacia do Amazonas*. Doctoral thesis, University of São Paulo, São Paulo, Brazil.

Soares, E.A.A., Tatumi, S.H., Riccomini, C., 2010. OSL age determinations of Pleistocene fluvial deposits in central Amazonia. *Anais da Academia Brasileira de Ciências* **82**, 691–699.

Summerfield, M.A., 1991. *Global Geomorphology*. Wiley, New York.

Su, Z., Wang, E., Furlong, K.P., Shi, X., Wang, G., Fan, C., 2012. Young, active conjugate strike-slip deformation in West Sichuan: evidence for the stress–strain pattern of the southeastern Tibetan Plateau. *International Geology Review* **54**, 991–1012.

Sylvester, A.G., 1988. Strike-slip faults. *Geological Society of America Bulletin* **100**, 1666–1703.

Tassinari, C.C.G., Bettencourt, J.S., Geraldes, M.C., Macambira, M.J.B., Lafon, J.M., 2000. The Amazon Craton. In: Cordani, U.G., Milani, E.J., Thomaz-Filho, A., Campos, D.A. (Eds.), *Tectonic Evolution of South America*. 31st International Geological Congress, Rio de Janeiro, Brazil, pp. 41–95.

Tebbens, S.F., Cande, S.C., 1997. Southeast pacific tectonic evolution from early Oligocene to Present. *Journal of Geophysical Research* **102**, 12,061–12,084.

Valeriano, M.M., Rossetti, D.F., 2008. Topographic modeling of Marajó Island with SRTM data. *Revista Brasileira de Geomorfologia* **9**, 53–63.

Valeriano, M.M., Rossetti, D.F., 2017. Regionalization of local geomorphometric derivations for geological mapping in the sedimentary domain of central Amazônia. *Computers and Geosciences* **100**, 46–56.

Val, P., Silva, C., Harbor, D., Morales, N., Amaral, F., Maia, T., 2013. Erosion of an active fault scarp leads to drainage capture in the Amazon region, Brazil. *Earth Surface Processes and Landforms* **39**, 1062–1074.

Veloso, A.V., 2014. On the footprints of a major Brazilian Amazon earthquake. *Anais da Academia Brasileira de Ciências* **86**, 1115–1129.

Walker, W.S., Kellndorfer, J.M., Pierce, L.E. 2007. Quality assessment of SRTM C- and X-band interferometric data: implications for the retrieval of vegetation canopy height. *Remote Sensing of Environment* **106**, 428–448.

Wanderley Filho J.R. 1991. Evolução estrutural da bacia do Amazonas e sua relação com o embasamento. M.Sc. thesis, Universidade Federal do Pará, Belém, Brazil.

Wessel, P., Smith, W.H.F., Scharroo, R., Luis, J.F., Wobbe, F., 2013. Generic mapping tools: improved version released. *EOS Transactions American Geophysical Union* **94**, 409–410.